Drug Synergy Screen and Network Modeling in Dedifferentiated Liposarcoma Identifies CDK4 and IGF1R as Synergistic Drug Targets

Martin L. Miller[1], **Evan J. Molinelli**[1,2], **Jayasree S. Nair**[3], **Tahir Sheikh**[3], **Rita Samy**[1], **Xiaohong Jing**[1], **Qin He**[1], **Anil Korkut**[1], **Aimee M. Crago**[4], **Samuel Singer**[4], **Gary K. Schwartz**[3,5], and **Chris Sander**[1]

[1]Computational Biology Center

[2]Tri-Institutional Training Program in computational Biology and Medicine

[3]Laboratory of New Drug Development, Department of Medicine

[4]Sarcoma Disease Management Program, Department of Surgery

[5]Melanoma and Sarcoma Service, Department of Medicine, Memorial Sloan-Kettering Cancer Center

Abstract

Dedifferentiated liposarcoma (DDLS) is a rare but aggressive cancer with high recurrence and low response rates to targeted therapies. Increasing treatment efficacy may require combinations of targeted agents that counteract the effects of multiple abnormalities. To identify a possible multicomponent therapy, we performed a combinatorial drug screen in a DDLS-derived cell line and identified cyclin-dependent kinase 4 (CDK4) and insulin-like growth factor 1 receptor (IGF1R) as synergistic drug targets. We measured the phosphorylation of multiple proteins and cell viability in response to systematic drug combinations and derived computational models of the signaling network. These models predict that the observed synergy in reducing cell viability with CDK4 and IGF1R inhibitors depend on activity of the AKT pathway. Experiments confirmed that combined inhibition of CDK4 and IGF1R cooperatively suppresses the activation of proteins within the AKT pathway. Consistent with these findings, synergistic reductions in cell viability were also found when combining CDK4 inhibition with inhibition of either AKT or epidermal growth factor receptor (EGFR), another receptor similar to IGF1R that activates AKT. Thus, network models derived from context-specific proteomic measurements of systematically perturbed cancer cells may reveal cancer-specific signaling mechanisms and aid in the design of effective combination therapies.

INTRODUCTION

Liposarcoma is the most common type of soft tissue sarcoma (1). Among the subtypes of liposarcoma, dedifferentiated liposarcoma (DDLS) is associated with the lowest survival rate (2) and often recurs or metastasizes despite treatment with surgery, radiation, or chemotherapy (3). As response rates to classical chemotherapeutics are low (4), targeted agents have increasingly been under pre-clinical and clinical investigation for DDLS treatment (3). Unfortunately, drugs directed to kinases such as vascular endothelial growth factor receptor (VEGFR), platelet-derived growth factor receptor (PDGFR) (for example, sorafenib), and BCR-ABL (for example, imatinib) show limited response in phase II trials (5, 6). Profiling of DDLS reveals complex DNA copy number changes across the genome as well as recurrent focal alterations, including a high frequency (~90%) 12q13-15 amplification that harbors the *CDK4* and *MDM2* oncogenes (7), which respectively encode cyclin-dependent kinase 4 (also known as cell division kinase 4) and mouse double minute 2 homolog, an E3 ubiquitin ligase. We previously evaluated the selective oral inhibitor of CDK4 and CDK6 (from here on referred to simply as CDK4), PD0332991, in a phase II clinical trial in patients with well-differentiated liposarcoma (WDLS) and DDLS and found prolongation of progression-free survival (8). However, the response rate remains low, suggesting that PD0332991 needs to be combined with other drugs to enhance its anti-tumor

efficacy, exemplified by the advances in treatment of estrogen receptor-positive and human epidermal growth factor receptor 2-negative (ER+/HER2−) advanced breast cancer with PD0332991 and the aromatase inhibitor Letrozole (clinical trial number NCT01740427).

Targeted therapies are revolutionizing cancer treatment by acting on patient-specific genetic alterations with fewer side effects than conventional cytotoxic chemotherapy. Despite these advantages, single-target therapies for cancer often have limited clinical success because of resistance, such as with HER2-targeted therapies for breast cancer (9, 10). In the case of limited initial treatment response (referred to as primary resistance), combination therapy with two or more targeted drugs improves efficacy (11, 12), such as the combination of the HER2-specific antibody trastuzumab with the receptor tyrosine kinase (RTK) inhibitor Lapatinib in HER2-positive metastatic breast cancer (13). Ongoing clinical trials with combination therapies include BRAF and MEK [mitogen activated kinase (MAPK) kinase] inhibition for *BRAF* mutant melanoma (clinical trial number NCT01072175) (14), phosphoinositide-3 kinase (PI3K) and MEK inhibition for *PIK3CA*/*KRAS* mutant colorectal cancer (clinical trial number NCT00996892), and AKT and MEK inhibition for advanced solid tumors (clinical trial number NCT01021748). The improvements of combination therapy are most likely because of cooperative inhibition of the multiple cellular signaling events typically altered in cancer (15–17). In DDLS, for example, in addition to the *CDK4* and *MDM2* amplicon, there are complex genetic rearrangements, including partial deletion of chromosomes 11q and 19q, suggesting that several dysregulated pathways are likely involved in DDLS pathogenesis (18, 19). Targeting multiple pathways with combinations of drugs therefore represents a relevant strategy for DDLS treatment and could potentially lead to higher response rates and better clinical outcomes. Moreover, by targeting two different pathways converging on a common phenotype, such as cell proliferation, it is possible to obtain a more-than-additive (synergistic) response compared to the individual agents alone (15, 20), sometimes referred to as the parallel pathway inhibition model (17, 21, 22). Synergistic drugs have the potential to not only increase the rate of initial treatment response (16, 23), but also reduce the concentration of each needed to elicit a given effect and consequently improve the therapeutic index (24).

The issue of how best to optimize drug combinations becomes particularly acute in developing combinations of drugs that have distinct cell cycle effects. In a process termed cell cycle-mediated drug resistance, a cell cycle inhibitor that blocks cell growth in one phase of the cell cycle (such as G1) can then antagonize a second drug that exerts its cytotoxic effect within another phase of the cell cycle (such as mitosis) (25). For example, the pan-CDK inhibitor flavopiridol, which induces a G1 cell cycle arrest, essentially prevents mitotic spindle poisons such as paclitaxel or docetaxel from exerting their anti-tumor effects during mitosis (26, 27). A similar inability to enhance the effect of cell cycle-specific chemotherapies is shown for the CDK4 inhibitor PD0332991 (28). Thus, combinations of cell cycle inhibitors with conventional chemotherapy or with small-molecule inhibitors that could similarly affect the cell cycle are not intuitive.

With the goal of identifying effective, synergistic drug combinations for DDLS treatment, we performed a synergy screen with fourteen targeted drugs in a cell line derived from a DDLS patient with the 12q13-15 amplicon. Out of several identified synergistic drug pairs,

we focused on an unexpected synergy observed with paired CDK4 and IGF1R inhibition. To investigate the possible mechanisms underlying this synergy, we applied our recently developed hybrid experimental and computational approach for deriving context-specific signaling models (29, 30). In a three-step process we: 1) performed combinatorial drug perturbations and used high-throughput reverse-phase protein arrays (RPPA) to measure the response of a panel of thirteen proteins and phosphoproteins, 2) derived network models based on the perturbation profiles and prior knowledge of signaling pathways, and 3) quantitatively simulated the effects of perturbations on signaling events through our models. The network model was used to predict the key regulatory proteins mediating the synergy, which were then assessed experimentally. Although our cell line-specific models may not be generalizable to other contexts, our results illustrate the potential for computationally assisted design and analysis of systematic perturbation screens to efficiently explore therapeutically relevant drug combinations. We anticipate that such integrated approaches to combinatorial therapeutics may provide translational opportunities for further development of DDLS treatment.

RESULTS

Drug combination screen identifies synergistic drug targets in DDLS

To investigate synergistic drug interactions in DDLS, we selected a tumor-derived cell line, DDLS8817, which contains several genomic alterations characteristic of DDLS, including amplification of 12q13-15 and partial loss of segments in chromosomes 3p and 19q (19) (fig. S1). We then chose fourteen small-molecule drugs (table S1 and Fig. 1) that target proteins within the canonical mTOR (mammalian target of rapamycin), PI3K/AKT, and MAPK pathways, which are altered across a wide range of cancers (31). In addition, some of these drugs are under preclinical and clinical investigation for treatment of various sarcoma subtypes, including drugs targeting CDK4 (8), PDGFR (platelet-derived growth factor receptor) (5), and IGF1R (32), although only partial therapeutic responses have been observed.

To determine potential non-additive effects (indicating the existence of common mechanisms, known as epistasis), the activity of combined agents is typically compared to single agent activities and related to a null expectation model that assumes no interaction between the drugs (24). The most commonly used null expectation models are Loewe additivity and Bliss independence (15), whereby effects can be categorized as additive, synergistic, or antagonistic. For this study, we measured synergy by the Loewe additivity-based combination index (CI) score, which can handle cases where two drugs act on targets regulating a common pathway (33) (Fig 1A). We then performed a systematic dose-response screen of single and combined agents at seven different concentrations administered for 72 hours and estimated the effect on cell viability using metabolic activity-based Resazurin assay. Using more than 10,000 cell viability measurements of the effect of all single and dual drug perturbations (table S2), CI scores were calculated for each drug combination on the basis of half-maximal effective concentration (EC_{50}) values obtained from sigmoid-fitted dose-response curves (Fig. 1B and fig. S2). CI scores less than 0.75 were considered synergistic, larger than 1.5 antagonistic, and the rest were considered additive (Fig. 1B and

table S3). In some cases, CI scores could not be calculated; for example, the mTOR inhibitor rapamycin arrested cells in a dose-independent manner. Using these CI score cut-offs, we identified 9 synergistic drug-drug interactions (out of a possible 91), which corresponds with previous reports in which 4–10% of the combinations were synergistic (34–37). The synergistic pairs included combined inhibition of epidermal growth factor receptor (EGFR) and IGF1R, MEK and either PI3K or AKT, among others [inclusively, AKT and MEK, ERK and HDAC (histone deacetylase), ERK and MET, IGF1R and CDK4, IGF1R and EGFR, IGF1R and STAT3 (signal transducer and activator of transcription 3), MEK and MET, PDGFR and MEK, PI3K and MEK].

CDK4 and IGF1R are synergistic drug targets in DDLS

We decided to further investigate the particular combination of CDK4 and IGF1R inhibition using the small molecules Ryuvidine and AG538 because of the recurrent CDK4 amplicon in DDLS and the clinical relevance of CDK4 inhibition for treatment of liposarcoma. In addition, the IGF1R target was a surprising combination candidate with CDK4 inhibition, because the two molecules are generally presumed to control cell survival through separate pathways [the AKT/mTOR pathway by IGF1R, and the retinoblastoma (RB) pathway by CDK4].

We first tested whether the main drug targets were driving the identified synergy and whether it was exclusive to the DDLS8817 cell line. To investigate this, we used alternative inhibitors, PD0332991 (a CDK4 inhibitor) and R1507 (an IGF1R antibody) in two DDLS cell lines, DDLS8817 and LPS141 (fig. S1 and table S4). Mixing serial dilutions of R1507 and PD0332991 in all combinations (dose matrix) and measuring their effect on cell metabolic activity (as an indication of cell viability) after 6 days of drug treatment, we calculated CI scores using CompuSyn (38), and found that these drugs were synergistic in both cell lines (average CI scores were 0.34 ± 0.19 for DDLS8817 and 0.63 ± 0.17 for LPS141) (Fig. 2). In addition, the IGF1R small molecule inhibitor NVP-AEW541 appeared to be synergistic in combination with PD0332991, although this was more prominent for LPS141 than for DDLS8817 (fig. S3) most likely because of a higher baseline abundance of IGF1R in LPS141. Finally, in LPS141, PD0332991 but not IGF1R inhibition alone (neither by inhibitor NVPAE nor by antibody R1507) induced G1 cell cycle arrest, with greater effects from combined treatment (fig. S4). These results indicate that the synergy of CDK4 and IGF1R inhibitors is most likely mediated by inhibition of the main targets rather than off-target effects, and support the findings of our initial screen in an independent cell line and with different agents targeted to the same molecules.

RPPA assay provides proteomic profiles for DDLS-specific network modeling

We next investigated possible mechanisms underlying the observed CDK4 and IGF1R inhibitor synergy by building network models of signaling pathways in DDLS. The approach consisted of profiling the cellular response (proteomic and phenotypic measurements) to a series of drug-pair perturbations, followed by computational transformation of the data into network models that quantitatively link proteins in signaling network circuits (29, 30).

For the first profiling step, we used the same cell line and the same set of drugs as in our initial drug synergy screen. In an effort to reveal interactions at relatively low doses, we selected drug concentrations that inhibited phosphorylation of the presumed target by 40% (IC_{40}) at 24 hours (fig. S5–S6 and table S1). Of note, the protein IC_{40} values used here were roughly one order of magnitude lower than the drugs' IC_{40} values for cell viability.

We then treated DDLS8817 cells with all individual drugs and all possible pairs of drugs, resulting in a total of 105 different perturbations, not counting biological replicates and untreated controls (Fig. 3A). Biological replicates of cellular lysates were spotted in 5-fold dilution series using the RPPA platform, and the abundance of more than 100 different proteins and phosphoproteins were assessed with a panel of antibodies (39). A final set of 13 antibodies was chosen for read-outs based on quality control of slides, correlation between biological replicates, response to drug perturbation, and evidence of the protein being relevant for liposarcoma tumor biology (Fig. 3B). This final set of antibody read-outs shows the overall pattern of increased (green) and decreased (blue) phosphoprotein abundance over the range single and dual drug perturbations. Several consistent patterns emerge across similar drug conditions (horizontal "bars", such as repression of phosphorylated AKT (at Ser^{473}) in the majority of drug pairs with the AKT inhibitor (conditions 15–27) as well as repression of phosphorylated MAPK (at Thr^{202}) with pairs of drugs that include ERK inhibition (conditions 28–39) or EGFR inhibition (conditions 40–50). Although difficult to interpret without computational analyses, distinct vertical patterns also appear, such as repression of multiple phosphoproteins with combined MEK and PI3K inhibition (condition 74) – a drug combination that was also found to have a synergistic reduction in cell viability (Fig. 1B). We tested the selected set of RPPA antibodies using Western blotting and found no apparent cross-reactivity to non-target antigens in the cell lines used (fig. S7). In addition, we profiled the two cell lines for mRNA expression using microarrays and found that the expression of the network genes ranked in the top half of all genes (fig. S8). Finally, we found multiple DNA copy numbers gains in the network genes and no homozygous deletions were detected (fig. S9). Together these observations on transcript, copy number, and protein abundance indicate that all selected genes were expressed at "steady state" in unperturbed conditions.

Proteomic data and prior knowledge interactions provide quantitative models of signaling pathways in DDLS

For inferring DDLS-specific network models, we utilized existing information on protein interactions from several databases (40–42) and information on signaling pathways involved in sarcoma (18). With this information, we constructed a prior knowledge network of interactions (termed edges) between the selected set of proteins measured by RPPA (termed nodes) (Fig. 4A and table S5). For simplicity, we represented the combined effects of cell proliferation, survival, and death as a single node (cell viability).

We next derived quantitative network models using three types of data: the perturbation-response profiles (Fig. 3B), the drug-target relationships (table S1), and the list of prior knowledge interactions (Fig. 4A). To maintain flexibility to infer interactions that are consistent with the experimental data, we softly enforced the prior knowledge interactions,

such that inconsistent interactions could be rejected. We inferred interactions into a give 'target' node one at a time by searching the data for weighted subsets of possible "source" nodes that collectively co-vary with the target node. Technically, this was done by minimizing a bipartite cost function that penalizes 1) discrepancies between model-predicted and measured values and 2) a large number of interactions. In this way, edges are numerical parameters representing the relative influence of one node on the state of another, representing logical but not necessarily direct biological interactions. Explicitly searching all possible subsets of source nodes is computationally prohibitive due to combinatorial explosion of possibilities. Therefore, we used a statistical inference algorithm called Belief Propagation (BP), which is designed to find the most probable interactions in large systems (30) (described in fig. S10). The output of the BP method is a probability distribution for each of the N^2 possible parameters, which we used to collect an ensemble of network models with the most probable interactions.

To visualize the inferred ensemble of network models, we plotted all of the highly probable interactions, with the edge width representing the inferred interaction strength (Fig. 4B). Qualitatively, we observed a fairly complex network of interactions with several phospho-proteins acting as hubs [for example, AKT at pSer[473], p70S6 kinase (p70S6K) at pThr[389], and glycogen synthase kinase α and β (GSK3α/β) at pSer[21]] and without any obvious modular or isolated pathways. The majority of the prior knowledge interactions (26 of 34) were consistent with the data (fig. S11) and were within the inferred network. Supporting this, models based on prior knowledge alone performed better than random models as estimated by the mean squared error between measured and model estimated data points (fig. S12). The rejected interactions were mostly those connecting the drugs (represented as activity nodes; for example, aPDGFR) to their presumed targets. Although some of this discrepancy may result from use of low drug concentrations, in some cases the measured phosphorylation site may not be affected by drug treatment despite the target being inhibited (for example, the abundance of phosphorylated MEK may not be affected by a MEK inhibitor). Although drug specificity is crucial for accurate network modeling, we found that off-target effects could be tolerated (fig. S13). Thus, using our network inference approach, we developed context-specific DDLS network models that can be used to simulate effects of perturbations.

Network models are predictive of cellular responses to drugs

To use the models for prediction, a collection of quantitative models were generated via sampling the probability distributions for each parameter and subsequently optimizing with a gradient descent method. Out of a collection of 1000 distinct network models, we then used the 100 best performing models (lowest error) to estimate how well the models quantitatively link nodes (measured proteins) in the network to the cell viability node. To assess this in our models, an inhibitory perturbation (single or paired) was simulated by applying a negative force on the target node(s), which in turn propagated changes to all other linked nodes sequentially, thus simulating a cascade of signaling events. To avoid over-fitting this test was performed using a cross-validation procedure in which we generated network models, where all measurements of paired drug perturbations involving the drug in question were left out (using "leave-k-out" cross-validation). We found that the

network modeling approach was reasonably accurate in predicting the effect of any pairwise node perturbation on cell viability (fig. S14). This indicated that central signaling connectivities were captured in a biologically relevant manner, because the predicted cell viability outcome depends on how information is propagated in the network models.

Network models capture synergy and recapitulate the CDK4 and IGF1R inhibitor synergism

We next investigated if the network models were able to identify epistatic (synergistic and antagonistic) interactions in the data. Applying a similar leave-k-out approach, possible epistatic effects on cell viability were determined by inhibiting two nodes at various strengths in all permutations. We determined epistatic effects in the network models, synergy (S), as the difference between the effect of the paired simulated perturbations (Z_{sim}) and the Loewe additivity surface (Z_{loewe}); $S = A,B$ (Z_{sim} Z_{loewe}), where Z_{loewe} was derived from the added effects of the single node perturbations (43). For example, when applying this approach to investigate the effects of combined inhibition of the ERK activity (aERK) and 4EBP1-pSer[65] nodes, we find that cell viability is inhibited more than expected over the additive independence model (Fig. 5A and B). Although it was not experimentally tested, this epistatic interaction was derived non-trivially from the input data and shows the ability to model and predict new potential synergistic drug targets. We then calculated S for all possible node pairs and found that our network models were able to capture epistasis as numerous synergistic and antagonistic effects were identified (Fig. 5C). Although S is unitless and can be used only for comparisons within the same dataset, the overall trend of the distribution is similar that found experimentally (Fig. 1B). This indicates that the modeling approach is not over- or underestimating synergistic effects; however, further efforts are needed to confirm this observation. We then compared predicted versus experimentally tested drug combinations. Although there were several miscategorized predictions, many of the drug combinations with the strongest predicted synergistic and antagonistic effects were categorized in accordance with the experiments (fig. S15).

Similar to the experimental results, the network models predicted a synergistic effect from combined inhibition of IGF1R and CDK4 (Fig 5C, fig. S16). Although the predicted efficacy, unlike the experimental synergy, was relatively modest, it was significantly different from synergy scores determined from perturbing the same nodes in random but similarly parameterized models (fig. S16C). Thus, the models effectively recapitulated the phenotypic observations for combined CDK4 and IGF1R inhibition.

Models predict that the AKT pathway is involved in mediating CDK4-IGF1R drug synergy

In an effort to identify important network features mediating the synergy of IGF1R and CDK4 inhibition, we systematically altered the network models to find the interactions that were essential for the synergistic effect on the cell viability node. Each interaction observed in at least one of the top 100 models was removed in turn, then the synergy calculation was repeated. The interactions whose removal resulted in the most pronounced drop in the overall synergy score were ranked (Fig. 6). This analysis yielded several important insights. First, most of the model interactions did not contribute to the synergy. Second, in agreement with the parallel pathway hypothesis model for drug synergy (17, 21, 22), the most

important interactions formed two seemingly parallel and non-overlapping pathways controlling cell viability. The most essential interactions were those linking the drug targets (aCDK4 and aIGF1R) to cell viability either directly or through downstream effectors such as RB-pSer^{780} (for aCDK4) and S6-pSer^{235} (for aIGF1R). Although some of these interactions are likely indirect and did not occur in the average network, they do represent strong causal connection between the drug-target and the predicted control over cell viability. In addition, this analysis suggested that control of the phosphorylation of AKT at Ser^{473} by activated EGFR (phosphorylated at Tyr^{992}) also plays an important role in mediating the synergy. The connections between AKT-pSer^{473}, p70S6K-pThr^{389}, S6-pSer^{235}, and cell viability, represent the canonical AKT/mTOR-pathway cascades regulating cell proliferation (44, 45) and are consistent with IGF1R-mediated cell proliferation regulation through this pathway. These predictions suggested that AKT was involved in mediating part of the observed synergy. Therefore we decided to investigate this in further detail.

AKT pathway-mediated control over cell viability is likely involved in the CDK4 and IGF1R inhibitor synergy

To begin interrogating the molecular pathways that might explain the CDK4 and IGF1R inhibitor synergy, we investigated effects of their inhibition on IGF1R, PI3K/AKT, and mTOR signaling in the two cell lines, DDLS8817 and LPS141. To address specificity issues, we used two IGF1R inhibitors (the IGF1R antibody R1507 and the small molecule IGF1R inhibitor NVP-AEW541) and the CKD4 inhibitor PD0332991 as well as CDK4-targeted siRNA. Under all of the conditions tested, the IGF1R inhibitor and antibody decreased the abundance of phosphorylated AKT (Fig. 7, A and B). With R1507, this decrease in phosphor-AKT was coincident with decreased IGF1R abundance, more markedly in LPS141 cells, which have a high baseline abundance of IGF1R. PD0332991 or CDK4 siRNA alone resulted in variable suppression of mTOR signaling with a decrease in both phosphorylated S6 (at Ser$^{235-236}$) and pS6K (at Thr^{389}) under some of the conditions tested. However, with the combination treatment of PD0332991 and R1507 there was evidence of enhanced inhibition of mTOR signaling indicated by decreased S6 phosphorylation (pSer$^{235-236}$) and S6K phosphorylation (pThr^{389}) (fig. S17B and C) as well as a similar, but non-significant, trend for suppression of phosphorylated AKT (fig. S17A). These data suggest that dual blockade of CDK4 and IGF1R signaling results in cooperativity such that two pro-survival pathways are inhibited. Despite the MAPK pathway being downstream of IGF1R, the same drug combination did not appear to cooperatively suppress the phosphorylation of ERK (Fig. 7A).

On the basis of these observations and our modeling results, we hypothesized that combining PD0332991 with inhibitors of the AKT pathway would also be synergistic. Indeed, measuring cell viability after 6 days of drug treatment, we found that combined AKT and CDK4 inhibition with MK2206 and PD0332991 resulted in a synergistic effect in both DDLS8817 and LPS141 (Fig. 7, C and D). Consistent with this, inhibiting EGFR, which is upstream of AKT, also synergized with PD0332991 (fig. S18A). In addition, in a triple drug perturbation, we observed cooperative effects of combining CDK4 inhibitor, IGF1R inhibitor, and EGFR inhibitor (fig. S18, B and C). In contrast, neither the MEK

inhibitor AZD6244 nor the ERK inhibitor FR180204 synergized with PD0332991, because the effects of these dual drug perturbations were comparable to single PD0332991 treatment (fig. S19), arguing that the MAPK pathway is not a point of convergence in the CDK4 and IGF1R inhibitor synergy. Taken together, these observations indicate that part of the synergistic mechanism may result from a more-than-additive suppression of phosphorylated AKT (at Ser[473]) and that the added anti-proliferative effect may involve inhibition of the AKT pathway rather than the MAPK pathway.

DISCUSSION

In this work we used a perturbation-based systems biology approach to analyze drug combination effects in DDLS. Performing a drug synergy screen in a patient-derived cell line, we identified CDK4 and IGF1R as synergistic drug targets. To investigate potential mechanisms of this synergy, we applied an integrated experimental-computational approach to infer network models from rich perturbation response profiles. We used these network models to quantitatively describe signaling pathways in DDLS and model the observed CDK4-IGF1R drug synergy. Both predictions and experiments suggest that AKT or effectors of AKT are involved in mediating this more-than-additive effect. Although other mechanisms are likely involved and further methodological developments are needed, these results reveal the power of network pharmacology approaches for identifying and modeling drug synergy.

Several features of this work may contribute substantially to the discovery and analysis of effective combination therapies. We have extended the conventional drug synergy screening approach by combining cell viability measurements with high-throughput proteomic measurements of systematically perturbed cancer cells. This enables us to apply our powerful probability-based BP algorithm to derive network models that integrate both prior knowledge of pathways and direct measurements of signaling events in the system of interest. In this way, we infer network models of signaling connectivities in a context-specific manner. This integrated experimental-computational approach is predictive of cell viability outcome to network perturbations and allows for modeling and predicting mechanisms of synergistic drug combinations, which is typically not possible with other approaches. Although the generalizability of our models remains untested, our approach is generalizable to other contexts, and we are currently modeling oncogenic signaling in several additional cancer types.

The applicability of our approach is exemplified by the discovery and modeling of the CDK4 and IGF1R drug synergy. Increasing evidence points to CDK4 as a major oncogenic driver in DDLS (7, 18, 19), however, because IGF1R is not frequently altered in DDLS (7), this drug combination would not likely be identified using standard genomic screening methods. On the basis of these results, we are continuing preclinical investigations in DDLS with paired CDK4 and IGF1R inhibition as well as devising clinical trials with multicomponent therapy consisting of PD0332991 combined with either IGF1R or EGFR inhibition. Both experiments and model simulations indicate that CDK4 and IGF1R inhibitors operate through separate survival pathways (through RB and AKT/mTOR, respectively) supporting the parallel pathway hypothesis for synergism (17, 21, 22). In this

light, we expect that the combination therapies suggested here may improve response rates in the initial treatment phase and thereby reduce primary resistance. Moreover, because CDK4 inhibition but not IGF1R blockade arrests cells in G1 (fig. S4), this particular combination may avoid problems of cell cycle-mediated drug resistance (25).

The network models predicted that regulation of AKT's effect on cell viability is critical for the observed CDK4 and IGF1R drug synergy. The AKT pathway is one of the major downstream pathways of IGF1R (46), and indeed we found that IGF1R inhibition with R1507 or NVP-AEW541 represses phosphorylation of AKT and downstream members of the AKT/mTOR pathway (p70S6K, S6). Consistent with the literature, CDK4 inhibition repressed phosphorylated RB (Fig. 7A) and had little to no repressive effect on the AKT/mTOR pathway by itself. However, the mTOR pathway was cooperatively repressed by paired inhibition of CDK4 and IGF1R compared to single treatment alone and a similar trend was observed for the AKT pathway (fig. S17). While AKT is known as an upstream regulator of cyclin D1 and CDK4 activity (47), CDK4 does not, to our knowledge, directly control AKT pathway activity. In this light, it is surprising that the paired perturbation has a more-than-additive suppressive effect on this pathway. This suggests the existence of an unknown connectivity or feedback mechanism, although further research is required to evaluate this idea. In accordance with the premise that the control of the AKT pathway contributes to the CDK4 and IGF1R inhibitor synergy, we found that combined inhibition of CDK4 and AKT or its upstream regulator EGFR resulted in a synergistic repression of cell proliferation. In contrast, combining CDK4 inhibition with either MEK inhibition or ERK inhibition showed no cooperative effects, eliminating the MAPK pathway by itself as a mechanism driving the synergy.

Designing the experimental setup for large-scale profiling, as performed here, requires a range of choices with respect to cell-type, growth conditions, drug selection, drug concentrations, assays, and so on. We chose clinically relevant cell lines and drugs for this study. However, some of the drugs used in the screen were not identical to those under preclinical development. For example, we used the CDK4 inhibitor ryuvidine in the synergy screen instead of the more specific and clinically relevant PD0332991. We found greater synergy with PD0332991 and R1507 than with ryuvidine and AG538, possibly reflecting differences in specificities. Similarly, the CDK4-AKT synergy and the CDK4-EGFR synergy were not observed in the original screen in which the CDK4 inhibitor was ryuvidine (Fig. 1B), but were observed in the follow-up experiments using PD0332991 (Fig. 7, C and D). Differences in the experimental setup, including different time points (3 versus 6 days) and different drug specificities, may explain some of this discrepancy. Another choice in the experimental design was in the determination of drug concentrations for the RPPA-based protein profiling, which was done on the basis of changes in the abundance of drug target proteins detected by Western blot. Ideally, the RPPA-assay itself should be used for this purpose, because targets of certain drugs elicited only moderate responses, possibly because of sensitivity differences between RPPA and Western Blot.

Increasingly, there is a demand for developing data-driven network inference algorithms that link signaling events to phenotypic outcomes (17, 48). Our modeling approach falls in between fully parameterized mass action kinetic models (49, 50) and "black box" machine-

learning models (51), offering significant predictive power while maintaining biological interpretability (30). We utilize probability distributions for each possible model interaction, calculated from an iterative BP algorithm, and thereby identify likely interactions and parameterize hundreds of predictive models. The ability to quickly construct these models frees us from relying on a single model and enables us to attach probabilities to predicted outcomes and construct alternative hypotheses. For example, multiple models (20 of the 100 lowest-error models) predicted strong synergy when inhibiting the CDK4 and IGF1R nodes (fig. S20). Although these 20 models may differ in some predicted outcomes, they all predicted that tight control of AKT from IGF1R inhibition and other upstream regulators is essential for the observed synergism.

For deriving DDLS network models, we incorporated existing background knowledge of protein interactions as it 1) reduces the search space of all possible interactions, 2) enables capturing cascades of signaling events with finer granularity, and 3) facilitates assigning directionality between correlated events. However, heavy restrictions from prior knowledge come with disadvantages. For example, common protein interactions described in other contexts may not exist in the system of interest. To balance between the use of prior knowledge and the ability to infer new interactions, we use flexible constraints so our method is able to accept or reject each prior knowledge interaction based on its fit with the experimental data and the inferred parameters. For example, an edge between phosphorylated RB (pSer^{807}-RB) and cell viability was encoded as a prior knowledge interaction but was not present in the average of the 1000 network models. The lack of identification of this interaction could possibly result from technical issues with the RPPA assay, low drug concentration, or off-target effects of ryuvidine. However, this edge was present in 49 of the top 100 models and thus narrowly missed being an average interaction, showing the importance of using an ensemble of models and not a single averaged model. Nevertheless, in our follow-up experiments, we recapitulated the CDK4-RB interaction as RB (phosphorylated at Ser^{780} and Ser^{807}) was suppressed by PD0332991 and by CDK4-directed siRNA (Fig. 7A). We found that the selected set of prior knowledge interactions enhanced model performance (fig. S12), but at the same time the models were not overfit to prior information (fig. S11). We realize that the final selection of prior knowledge interactions is qualitative and additional known interactions could have been included for better performance. However, in our case the performance of prior information alone was small compared to overall performance of BP-derived models trained on both data and prior knowledge (fig. S12 and table S6).

Drug specificity is a fundamental element of our modeling approach, and some of the drugs used in this work may have off-target effects. Whereas known off-target effects can directly be incorporated in to the modeling approach, unknown off-targets may pose challenges in interpretation and general predictive power of the network models. We found that lack of drug specificity does not prohibitively confuse the inference of interactions since the BP method can infer interactions from the correlations in the data itself (fig. S13). Hereby, our modeling strategy can effectively predict on-target, off-target, and/or indirect drug effects since each drug is represented in the models as an "activity node". Specificity is primarily a problem for predicting outcome of response to perturbation, since this requires knowing which elements are being perturbed for any drug. Nevertheless, we were able to correctly

predict the CDK4-IGF1R synergy outcome using models that were derived from perturbation data that included the CDK4 inhibitor Ryuvidine, which is known to have non-specific effects. In the future, we expect that by looking at response to different drugs acting on the same primary target, we can disambiguate signals that are due to changes in the known target from those that are due to off-target effects.

Our network modeling approach recapitulated the experimentally observed CDK4-IGF1R drug synergy as well as several of the strongest predicted non-additive combinations (fig. S15). However, several predictions were miscategorized. With the current modeling approach, we did not expect to accurately predict synergy. The major problem is that only cell viability measurements from one drug concentration (the one used in the RPPA screen) could be incorporated during model training, making it challenging to predict synergy from data obtained from two single drug and one drug-pair perturbations. On the experimental side, seven different concentrations for both single and paired drugs were used. Furthermore, the experimental synergies were determined using high drug concentrations while the models were trained to data collected from low drug concentrations (roughly 10-fold lower). These discrepancies were limitations with our experimental design and model implementation, which we expect to solve in future work. Other limiting factors for the miscategorizations include: 1) different measurement time point between the RPPA and the cell viability screen (24 versus 72 hours), 2) important regulators that were not measured and therefore absent from the derived networks, and/or 3) the experimental or computational approaches may have technical limitations. Future work will aim to address this by incorporating multiple doses and time-points. With further experimental and algorithmic improvements, the number of measured proteins in the networks can in principle be expanded to handle hundreds of nodes. Furthermore, the approach can be extended to predict synergy and mechanisms beyond the set of tested drugs. This is possible because all measured proteins, whether they are perturbed or not, become part of the network models. In this way, the set of possible predictions is further expanded to include any measured protein, enabling efficient computational screening and identification of combinatorial interventions.

This study was an interdisciplinary study to find clinically relevant drug combinations for treatment of DDLS, explore the use of computational modeling to predict synergistic or efficacious drug combinations, and identify biological mechanisms driving synergistic drug combinations. As our data indicate, our integrated approach has contributed with several advancements in these areas. For future studies, we are planning to further test and optimize the CDK4 and IGF1R drug combination as a potential DDLS treatment, while simultaneously developing the data-driven modeling strategy for predicting new drug targets and drug combinations.

MATERIAL AND METHODS

Cell lines and drugs

The LPS141 and DDLS8817 cell lines were derived from high-grade retroperitoneal dedifferentiated liposarcoma tumors (52). All cells were maintained in DMEM medium supplemented with antibiotics and 10% fetal bovine serum (FBS). A set of 14 small molecule drugs was selected for the drug synergy screen and RPPA proteomic assay with

DDLS8817 cells (table S1). For follow-up experiments with DDLS8817 and LPS141 cells, an additional 7 drugs were used (table S4).

DNA copy number and mRNA expression profiling

RNA and DNA from asynchronously growing DDLS8817 and LPS141 cultures were isolated with RNEasy and DNEasy kits per manufacturer's specifications (Qiagen). DNA copy number profiling was performed using the 244K Agilent array-comparative genomics hybridization (aCGH) platform, and standard circular binary segmentation (R/bioconductor DNAcopy library) was analyzed using the RAE algorithm (53). Transcript profiling was performed using the Illumina HT 12 V3 microarray platform and data was processed with the BeadStudio software version 3.3.7.

Resazurin cell viability assay

Although strictly a measure of cell metabolic activity, the resazurin assay is widely used as a measure of cell viability. DDLS8817 cells were seeded in 100 μL volume per well of 96-well plates (1000 cells/well) and grown for 24 hours. Cells were then inhibited with seven different concentrations (2 fold dilution) of single and dual drug agents in six replicates by adding 100 μL of drug solution per well. After 72 hours, resazurin (Sigma-Aldrich) was added to each well at a final concentration of 44 μM and incubated for 2–3 hours at 37°C. The fluorescent signals were measured with a SpectraMax microplate reader (Molecular Devices Corp.) using 530 nm excitation wavelength and 590 nm emission wavelength. Cell viability was normalized to control cells treated with drug vehicle (DMSO). The Resazurin assay measures mitochondrial metabolic activity and correlates well with the number of cells (54).

CCK-8 colorimetric cell viability assay

Similar to the resazurin assay, the CCK-8 assay measures cell metabolic activity and is widely used as a measure of cell viability. The assay was done as per the manufacturer's protocol (Dojindo Molecular Technologies, Inc.). Briefly, 1700 cells were plated in 100 μL volume per well of a 96-well plate, and treatments were done 24 hours after plating. After 3 or 6 days of drug treatment, 10 μL of CCK-8 solution was added to each well and further incubated at 37°C for 1 to 4 hours. This assay quantifies the amount of formazan dye generated by the activity of cellular dehydrogenases, which is directly proportional to the number of living cells. Cell viability was measured using Spectra Max 340 PC (Molecular Devices Corp.) with optical density at 450 nm.

siRNA transfection

500,000 cells were plated on 60-mm plates, and transfections using lipofectamine RNAiMAX (Invitrogen) were performed according to the manufacturer's protocol. CDK4 siRNA and control siRNA were purchased from Santa Cruz Biotechnology. Combination treatments with drugs were done 24 hours after transfection.

Flow cytometry

For cell cycle analysis cells were trypsinized, washed, and fixed in 75% ice-cold ethanol after 24 hours of drug treatment. Cells were stained with propidium iodide (50 μg/mL) containing RNase (5 μg/mL) for the measurement of DNa content. Samples were analyzed on a FACScan (Becton Dickinson) for cell cycle distribution using the Cell Quest software. For this analysis 10,000 events were examined per sample.

Protein extraction and immunoblotting

Cell lysates were prepared by lysing both floating and adherent cells in RIPA buffer [50 mmol/L Tris, pH 7.4, 150 mmol/L NaCl, 1% NP-40, 1 mmol/L EDTA, 0.25% Sodium deoxycholate, with protease inhibitor cocktail tablet (Roche)], allowed to lyse on ice for 10 min, syringed, and cleared by centrifugation in a microcentrifuge at 13,000 rpm for 10 min at 4°C. 25 μg protein was fractionated by SDS-PAGE and transferred onto Immobilon membranes (Millipore). Equal protein loading was confirmed by Amido black staining (Bio-Rad). After blocking with 5% nonfat milk, membranes were probed with primary antibodies. The following antibodies were used in this study: phosphorylated 4EBP1 (pSer[65]), phosphorylated AKT (pSer[473]), AKT, CDK4, GAPDH, GSK3α/β (pSer[9]/pSer[21]), IGF1R, phosphorylated EGFR (pSer[992]), phosphorylated MEK (pSer[217]), PKCα, phosphorylated RB (pSer[780]), phosphorylated RB (pSer[807]/pSer[811]), RB, phosphorylated S6 (pSer[235-236]), S6, phosphorylated S6K (pThr[389]), S6K, phosphorylated STAT3 (pTyr[705]), and phosphorylated SRC (pTyr[527]) from Cell Signaling Technology; phosphorylated ERK (pTyr[204]) and ERK from Santa Cruz Biotechnology. Bound primary antibodies were detected with horseradish peroxidase–conjugated secondary antibodies (GE Healthcare UK Limited) and visualized by enhanced chemiluminescence reagent (GE Healthcare UK Limited).

RPPA assay

Drug concentration for the RPPA screen were based on the IC_{40} of targets or downstream targets measured by Western blotting or based on information obtained from literature/manufacturer (table S1). IC_{40} was chosen in order to maximize the possibility of capturing synergistic and antagonistic effects of drug combinations while operating within the linear dynamic range of the antibody-based measurements. DDLS8817 cells were grown in 6-well plates to around 60% confluence. Cells were inhibited with drugs and harvested after 24 hours by collecting and freezing the cell pellet. Non-perturbed control cells were treated with drug vehicle (DMSO) for 24 hours. Cells were thawed, lysed and protein concentrations were determined by the Bradford assay (BioRAD). Protein concentrations were adjusted to 1–1.5 mg/mL and denatured in 2% SDS for 5 minutes at 95°C. Each condition was analyzed in duplicates from two independent biological samples. The RPPA assay was performed at the RPPA core facility at MD Anderson Cancer Center, where cell lysates were spotted on nitrocellulose-coated slides as described previously (39) and stained with approximately 100 different antibodies.

RPPA data analysis

The antibody staining intensities were quantified using the MicroVigene automated RPPA module (VigeneTech). Data handling consisted of correction of systematic spatial effects due to the location of the sample on the chip (55), conversion of dilution series to a single intensity readout (56), replicate averaging, and z-score scaling within each antibody readout. Z-score scaling was chosen as a normalization method as it robustly captures both activating and inhibiting effects over the entire series of perturbations (>600, including replicates, untreated controls, and additional drugs), and hereby minimizes the risk of systematic errors that may arise when normalizing to a subset of conditions, such as untreated controls. Supporting this, we found a better correlation between biological replicates when z-score normalizing compared to normalizing to untreated controls. After data handling, a subset of the total panel of antibody-stained chips was selected by first removing chips that were unevenly stained, saturated, or under exposed. Second, antibody readouts for which at least 10 conditions produced a z-score with an absolute value greater than one were retained. Finally, antibodies with a Pearson correlation coefficient above 0.5 between biological replicates or antibodies that were present in the prior knowledge network were selected.

Combination index score

Based on cell viability measurements, we used the combination index (CI) score to determine if two drugs had synergistic, antagonistic, or additive effects. The CI score is well suited for estimating effects of drug combinations as it is based on the concept of dose-substitution and can handle cases where the two drugs are the same, act on the same target, or act on targets converging in a common pathway (15). The CI score,

$CI_X = \frac{C_1}{EC_{X,1}} + \frac{C_2}{EC_{X,2}}$ measures the fractional shift between the combination doses (C_1 and C_2) and the single agent's inhibitory concentration for a given level of inhibition ($EC_{X,1}$ and $EC_{X,2}$). For this study, we used the half maximal effective concentration (EC_{50}), which was the drug concentration that induced a response halfway between the maximum and minimum observed effect of the condition with the largest inhibitory effect (either single or dual). To obtain a confidence estimate, CI scores were also calculated at EC_{45} and EC_{55} levels and standard deviations of the CI scores were reported (table S3). If a single agent did not reach the chosen effect level (% inhibition level of the condition with the largest effect), we assumed no effect of this drug and its contribution to the combination dose became negligible ($C_1 = 0$ and $C_1 = 0$). In cases where neither single nor dual perturbation resulted in an inhibitory effect less than 25% of control levels, CI scores were not determined and reported as "not a number" (NaN). For cell viability experiments where all mixtures of two serially diluted agents (dose matrix) were performed, CompuSyn was used for calculation of CI scores at various effect levels (38).

Network modeling

Cell viability in response to drug intervention is mediated through coordinated changes in the concentrations of proteins and phospho-proteins. We modeled these connected changes as a set of coupled nonlinear ordinary differential equations (ODEs) (fig. S7). Each model variable (or network node) represents the z-score of a biological entity, where the z-score is

a measure of significant change from the average abundance measurement across a large set of drug conditions from which 105 conditions were kept for modeling. Positive and negative values correspond to concentrations above and below the average response, respectively. Our models capture epistasis-like effects and the tendency of a system to return to the baseline state, which we observe to be nearly identical to the untreated as well as average condition. The dynamics are driven by perturbations represented as external forces (u_i) on one or more model variables (x_i), which drive the system of equations to a unique steady-sate. The steady state is taken to be the model predicted outcome to the perturbation.

We have incorporated the use of so-called "activity nodes", which represent the kinase activity of proteins (30). These activity nodes are introduced to distinguish between phosphorylated and active states of kinases. For example, MEK can be in a phosphorylated but not active state, where phosphorylated MEK does not propagate signals to its downstream effectors. In this example, kinase activity of MEK (aMEK) is altered with drugs but not directly measureable with antibody. Without readouts of activity, there is no evidence to determine regulators of such activity nodes. Consequently, all activity-nodes have only outgoing interactions and represent the points of entry of the various drugs on the network.

Network model parameterization

The models are fully parameterized by an N-by-N weigh matrix (W), which contains signed values (w_{ij}) representing an interaction from model variable x_j on to model variable x_i. Given that our model equations are abstractions from the underlying biochemistry of signaling events, we expect that multiple models can fit the collected dataset. We define a probabilistic description of model space that rewards fitness to experimental data and agreement with prior knowledge.

$$P(W)=e^{-\beta\sum_{i}^{N}\sum_{\mu}^{M}\left(x_i^{\mu^*}-x_i^{\mu}\right)^2}e^{-\lambda\sum_{i}^{N}\sum_{j\neq i}^{N}\delta(w_{ij})}$$

$$\delta(w_{ij})=\begin{cases} 0 & \text{if } w_{ij} \text{ is consistent with prior knowledge} \\ 1 & \text{if } w_{ij} \text{ is inconsistent with prior knowledge} \end{cases}$$

The experimental and simulated outcomes for a perturbation condition μ are denoted $x_i^{\mu^*}$ and x_i^{μ}. There are K^{N^2} possible configurations of this weight matrix, where K is the number of possible parameter assignments for a single interaction. Explicit calculation of this probability distribution is computationally prohibitive given the large number of possible model configurations.

Model construction

We adapted the BP inference method for approximating the probability distributions for each possible parameter (w_{ij}). A detailed description of our application of BP to perturbation data is provided elsewhere (30). We constructed 1000 high probability models by sampling from the BP-calculated probability distributions (fig. S7). We kept only the top 100 models

after parameter refinement with gradient descent (57) and ranking by performance metrics on the training set, and only these 100 low error models are used for direct simulation and prediction.

Average network models

We used an average network model for qualitative visual analysis of our inference results. An average model is simply the concatenation of all interaction parameters whose expected value from the BP probability distribution is non-zero. For this work, only average edges with interaction strength above or below 0.1 in the set of 1000 models were shown. Note that, average network models do not capture mutually exclusive interactions, as an average model may contain two interactions that never co-exist in the individual models. The sparsity of the networks is tunable through the parameter λ, such that larger values of λ yield sparser networks. In this work, we set λ and β equal to 2 and 3, respectively.

Leave-k-out cross validation

To estimate genuine power of our models to predict response to drug combinations, we partitioned the full dataset into a training set and test set. Test sets consist of all drug pair conditions involving a drug of interest, thereby leaving a training set consisting of all other conditions including the drug of interest applied alone. We constructed a unique set of 100 top performing models for a training set, with which we predict and compare against the withheld test set data.

Model prediction of cell viability outcome and synergy

We modeled single target inhibition with a constant external force (u_i as in the equation in fig. S7) on a single node in the interconnected system. Roughly, the value of the external perturbation is related to the expected deviation from average, such that the simulated effect of the cell viability node (E_{CV}) in the presence of inhibition of node A (x_{cv}^A) is expressed relative to 0 (average). To obtain synergy scores for a combination of inhibition of node A and B, we subjected the models to 8 increasing strengths of each perturbation and all 8-by-8 strength combinations. We estimated non-additive effects by calculating the difference between the simulated effects (Z_{sim}) and the Loewe additivity surface (Z_{loewe}), derived from adding the effects of single agent perturbations (43). The synergy score was taken to be the sum of the differences across all 8-by-8 conditions; $S = \sum_{A,B} (Z_{\text{sim}} - Z_{\text{loewe}})$. The unitless score, S, is only a relative measure of synergy and does not map directly to CI values. As our modeling approach does not explicitly incorporate drug concentrations, CI scores could not used as a synergy measure for the computed perturbation effects.

Supplementary Material

Refer to Web version on PubMed Central for supplementary material.

Acknowledgments

REFERENCES AND NOTES

1. Dei Tos A. Liposarcoma: New entities and evolving concepts. Annals of Diagnostic Pathology. 2000; 4:252–266. [PubMed: 10982304]

2. Jones RL, Fisher C, Al-Muderis O, Judson IR. Differential sensitivity of liposarcoma subtypes to chemotherapy. European Journal of Cancer. 2005; 41:2853–2860. [PubMed: 16289617]

3. Crago AM, Singer S. Clinical and molecular approaches to well differentiated and dedifferentiated liposarcoma. Current Opinion in Oncology. 2011; 23:373–378. [PubMed: 21552124]

4. Lorigan P, Verweij J, Papai Z, Rodenhuis S, Le Cesne A, Leahy MG, Radford JA, Van Glabbeke MM, Kirkpatrick A, Hogendoorn PCW, Blay J-Y. E. O. f. R. a. T. o. C. S. T. a. B. S. G. Study. Phase III trial of two investigational schedules of ifosfamide compared with standard-dose doxorubicin in advanced or metastatic soft tissue sarcoma: a European Organisation for Research and Treatment of Cancer Soft Tissue and Bone Sarcoma Group Study. Journal of Clinical Oncology. 2007; 25:3144–3150. [PubMed: 17634494]

5. Maki RG, D'Adamo DR, Keohan ML, Saulle M, Schuetze SM, Undevia SD, Livingston MB, Cooney MM, Hensley ML, Mita MM, Takimoto CH, Kraft AS, Elias AD, Brockstein B, Blachère NE, Edgar MA, Schwartz LH, Qin LX, Antonescu CR, Schwartz GK. Phase II study of sorafenib in patients with metastatic or recurrent sarcomas. Journal of Clinical Oncology. 2009; 27:3133–3140. [PubMed: 19451436]

6. Chugh R, Wathen JK, Maki RG, Benjamin RS, Patel SR, Meyers PA, Myers PA, Priebat DA, Reinke DK, Thomas DG, Keohan ML, Samuels BL, Baker LH. Phase II multicenter trial of imatinib in 10 histologic subtypes of sarcoma using a bayesian hierarchical statistical model. Journal of Clinical Oncology. 2009; 27:3148–3153. [PubMed: 19451433]

7. Barretina J, Taylor BS, Banerji S, Ramos AH, Lagos-Quintana M, DeCarolis PL, Shah K, Socci ND, Weir BA, Ho A, Chiang DY, Reva B, Mermel CH, Getz G, Antipin Y, Beroukhim R, Major JE, Hatton C, Nicoletti R, Hanna M, Sharpe T, Fennell TJ, Cibulskis K, Onofrio RC, Saito T, Shukla N, Lau C, Nelander S, Silver SJ, Sougnez C, Viale A, Winckler W, Maki RG, Garraway LA, Lash A, Greulich H, Root DE, Sellers WR, Schwartz GK, Antonescu CR, Lander ES, Varmus HE, Ladanyi M, Sander C, Meyerson M, Singer S. Subtype-specific genomic alterations define new targets for soft-tissue sarcoma therapy. Nature Genetics. 2010; 42:715–721. [PubMed: 20601955]

8. Dickson MA, Tap WD, Keohan ML, D'Angelo SP, Gounder MM, Antonescu CR, Landa J, Qin LX, Rathbone DD, Condy MM, Ustoyev Y, Crago AM, Singer S, Schwartz GK. Phase II Trial of the CDK4 Inhibitor PD0332991 in Patients With Advanced CDK4-Amplified Well-Differentiated or Dedifferentiated Liposarcoma. Journal of Clinical Oncology. 2013; 31:2024–2028. [PubMed: 23569312]

9. Saini KS, Azim HA Jr, Metzger-Filho O, Loi S, Sotiriou C, de Azambuja E, Piccart M. Beyond trastuzumab: New treatment options for HER2-positive breast cancer. The Breast. 2012; 20:S20–S27. [PubMed: 22015288]

10. Pohlmann PR, Mayer IA, Mernaugh R. Resistance to Trastuzumab in Breast Cancer. Clinical Cancer Research. 2009; 15:7479–7491. [PubMed: 20008848]

11. Jänne PA, Gray N, Settleman J. Factors underlying sensitivity of cancers to small-molecule kinase inhibitors. Nature reviews Drug discovery. 2009; 8:709–723.

12. Csermely P, Agoston V, Pongor S. The efficiency of multi-target drugs: the network approach might help drug design. Trends in Pharmacological Sciences. 2005; 26:178–182. [PubMed: 15808341]

13. Blackwell KL, Burstein HJ, Storniolo AM, Rugo H, Sledge G, Koehler M, Ellis C, Casey M, Vukelja S, Bischoff J, Baselga J, O'Shaughnessy J. Randomized Study of Lapatinib Alone or in Combination With Trastuzumab in Women With ErbB2-Positive, Trastuzumab-Refractory Metastatic Breast Cancer. Journal of Clinical Oncology. 2010; 28:1124–1130. [PubMed: 20124187]

14. Flaherty KT. Dividing and conquering: controlling advanced melanoma by targeting oncogene-defined subsets. Clinical and Experimental Metastasis. 2012

15. Fitzgerald JB, Schoeberl B, Nielsen UB, Sorger PK. Systems biology and combination therapy in the quest for clinical efficacy. Nature Chemical Biology. 2006; 2:458–466.

16. Glickman MS, Sawyers CL. Converting Cancer Therapies into Cures: Lessons from Infectious Diseases. Cell. 2012; 148:1089–1098. [PubMed: 22424221]

17. Al-Lazikani B, Banerji U, Workman P. Combinatorial drug therapy for cancer in the post-genomic era. Nature Biotechnology. 2012:1–13.

18. Taylor BS, Barretina J, Maki RG, Antonescu CR, Singer S, Ladanyi M. Advances in sarcoma genomics and new therapeutic targets. Nature Reviews Cancer. 2011; 11:541–557.

19. Crago AM, Socci ND, Decarolis P, O'Connor R, Taylor BS, Qin LX, Antonescu CR, Singer S. Copy Number Losses Define Subgroups of Dedifferentiated Liposarcoma with Poor Prognosis and Genomic Instability. Clinical Cancer Research. 2012; 18:1334–1340. [PubMed: 22241790]

20. Lehár J, Stockwell BR, Giaever G, Nislow C. Combination chemical genetics. Nature Chemical Biology. 2008; 4:674–681.

21. Cokol M, Chua HN, Tasan M, Mutlu B, Weinstein ZB, Suzuki Y, Nergiz ME, Costanzo M, Baryshnikova A, Giaever G, Nislow C, Myers CL, Andrews BJ, Boone C, Roth FP. Systematic exploration of synergistic drug pairs. Molecular Systems Biology. 2011; 7:1–9.

22. Yeh PJ, Hegreness MJ, Aiden AP, Kishony R. Drug interactions and the evolution of antibiotic resistance. Nature Reviews Microbiology. 2009; 7:460–466.

23. Azmi AS, Wang Z, Philip PA, Mohammad RM, Sarkar FH. Proof of Concept: Network and Systems Biology Approaches Aid in the Discovery of Potent Anticancer Drug Combinations. Molecular Cancer Therapeutics. 2010; 9:3137–3144. [PubMed: 21041384]

24. Greco WR, Bravo G, Parsons JC. The search for synergy: a critical review from a response surface perspective. Pharmacological reviews. 1995; 47:331–385. [PubMed: 7568331]

25. Shah MA, Schwartz GK. Cell cycle-mediated drug resistance: an emerging concept in cancer therapy. Clinical Cancer Research. 2001; 7:2168–2181. [PubMed: 11489790]

26. Motwani M, Delohery TM, Schwartz GK. Sequential dependent enhancement of caspase activation and apoptosis by flavopiridol on paclitaxel-treated human gastric and breast cancer cells. Clinical Cancer Research. 1999; 5:1876–1883. [PubMed: 10430095]

27. Motwani M, Li X, Schwartz GK. Flavopiridol, a cyclin-dependent kinase inhibitor, prevents spindle inhibitor-induced endoreduplication in human cancer cells. Clinical Cancer Research. 2000; 6:924–932. [PubMed: 10741717]

28. McClendon AK, Dean JL, Rivadeneira DB, Yu JE, Reed CA, Gao E, Farber JL, Force T, Koch WJ, Knudsen ES. CDK4/6 inhibition antagonizes the cytotoxic response to anthracycline therapy. Cell Cycle. 2012; 11:2747–2755. [PubMed: 22751436]

29. Nelander S, Wang W, Nilsson B, She Q-B, Pratilas C, Rosen N, Gennemark P, Sander C. Models from experiments: combinatorial drug perturbations of cancer cells. Molecular Systems Biology. 2008; 4

30. Molinelli EJ, Korkut A, Wang W, Gauthier NP, Jing X, Kaushik P, Miller ML, He Q, Weigt M, Pagnani A, Braunstein A, Zecchina R, Sander C. (Submitted).

31. Hanahan D, Weinberg RA. Hallmarks of Cancer: The Next Generation. Cell. 2011; 144:646–674. [PubMed: 21376230]

32. Olmos D, Martins AS, Jones RL, Alam S, Scurr M, Judson IR. Targeting the Insulin-Like Growth Factor 1 Receptor in Ewing's Sarcoma: Reality and Expectations. Sarcoma. 2011; 2011:1–13.

33. Chou TC, Talalay P. Quantitative analysis of dose-effect relationships: the combined effects of multiple drugs or enzyme inhibitors. Advances in enzyme regulation. 1984; 22:27–55. [PubMed: 6382953]

34. Zhang L, Yan K, Zhang Y, Huang R, Bian J, Zheng C, Sun H, Chen Z, Sun N, An R, Min F, Zhao W, Zhuo Y, You J, Song Y, Yu Z, Liu Z, Yang K, Gao H, Dai H, Zhang X, Wang J, Fu C, Pei G, Liu J, Zhang S, Goodfellow M, Jiang Y, Kuai J, Zhou G, Chen X. High-throughput synergy screening identifies microbial metabolites as combination agents for the treatment of fungal infections. Proceedings of the National Academy of Sciences. 2007; 104:4606–4611.

35. Farha MA, Brown ED. Chemical Probes of Escherichia coli Uncovered through Chemical-Chemical Interaction Profiling with Compounds of Known Biological Activity. Chemistry and Biology. 2010; 17:852–862. [PubMed: 20797614]

36. Yeh P, Tschumi AI, Kishony R. Functional classification of drugs by properties of their pairwise interactions. Nature Genetics. 2006; 38:489–494. [PubMed: 16550172]

37. Borisy AA, Elliott PJ, Hurst NW, Lee MS, Lehár J, Price ER, Serbedzija G, Zimmermann GR, Foley MA, Stockwell BR, Keith CT. Systematic discovery of multicomponent therapeutics. Proceedings of the National Academy of Sciences. 2003; 100:7977–7982.

38. Chou TC. Theoretical Basis, Experimental Design, and Computerized Simulation of Synergism and Antagonism in Drug Combination Studies. Pharmacological reviews. 2006; 58:621–681. [PubMed: 16968952]

39. Tibes R, Qiu Y, Lu Y, Hennessy B, Andreeff M, Mills GB, Kornblau SM. Reverse phase protein array: validation of a novel proteomic technology and utility for analysis of primary leukemia specimens and hematopoietic stem cells. Molecular Cancer Therapeutics. 2006; 5:2512–2521. [PubMed: 17041095]

40. Cerami EG, Gross BE, Demir E, Rodchenkov I, Babur O, Anwar N, Schultz N, Bader GD, Sander C. Pathway Commons, a web resource for biological pathway data. Nucleic Acids Research. 2010; 39:D685–D690. [PubMed: 21071392]

41. Ogata H, Goto S, Sato K, Fujibuchi W, Bono H, Kanehisa M. KEGG: Kyoto Encyclopedia of Genes and Genomes. Nucleic Acids Research. 1999; 27:29–34. [PubMed: 9847135]

42. Schaefer CF, Anthony K, Krupa S, Buchoff J, Day M, Hannay T, Buetow KH. PID: the Pathway Interaction Database. Nucleic Acids Research. 2009; 37:D674–D679. [PubMed: 18832364]

43. Lehár J, Krueger AS, Avery W, Heilbut AM, Johansen LM, Price ER, Rickles RJ, Short GF III, Staunton JE, Jin X, Lee MS, Zimmermann GR, Borisy AA. Synergistic drug combinations tend to improve therapeutically relevant selectivity. Nature Biotechnology. 2009; 27:659–666.

44. Chang F, Lee JT, Navolanic PM, Steelman LS, Shelton JG, Blalock WL, Franklin RA, McCubrey JA. Involvement of PI3K/Akt pathway in cell cycle progression, apoptosis, and neoplastic transformation: a target for cancer chemotherapy. Leukemia. 2003; 17:590–603. [PubMed: 12646949]

45. Vivanco I, Sawyers CL. The phosphatidylinositol 3-Kinase–AKT pathway in human cancer. Nature Reviews Cancer. 2002; 2:489–501.

46. Schlessinger J. Cell signaling by receptor tyrosine kinases. Cell. 2000; 103:211–225. [PubMed: 11057895]

47. Shimura T. Acquired Radioresistance of Cancer and the AKT/GSK3β/cyclin D1 Overexpression Cycle. Journal of Radiation Research. 2011; 52:539–544. [PubMed: 21881296]

48. Pe'er D, Hacohen N. Principles and strategies for developing network models in cancer. Cell. 2011; 144:864–873. [PubMed: 21414479]

49. Nakakuki T, Birtwistle MR, Saeki Y, Yumoto N, Ide K, Nagashima T, Brusch L, Ogunnaike BA, Okada-Hatakeyama M, Kholodenko BN. Ligand-Specific c-Fos Expression Emerges from the Spatiotemporal Control of ErbB Network Dynamics. Cell. 2010; 141:884–896. [PubMed: 20493519]

50. Aldridge BB, Burke JM, Lauffenburger DA, Sorger PK. Physicochemical modelling of cell signalling pathways. Nature Cell Biology. 2006; 8:1195–1203.

51. Chatterjee MS, Purvis JE, Brass LF, Diamond SL. Pairwise agonist scanning predicts cellular signaling responses to combinatorial stimuli. Nature Biotechnology. 2010; 28:727–732.
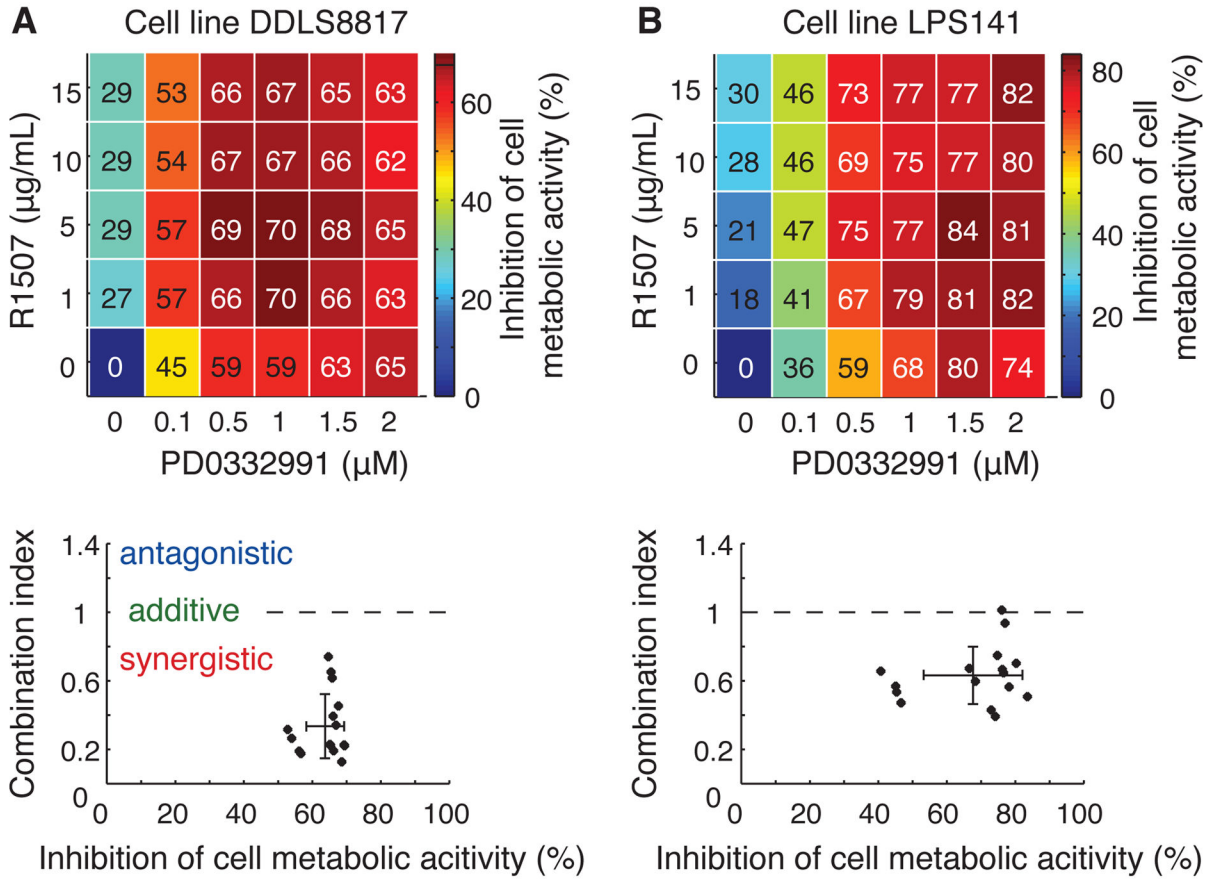
52. Singer S, Socci ND, Ambrosini G, Sambol E, Decarolis P, Wu Y, O'Connor R, Maki R, Viale A, Sander C, Schwartz GK, Antonescu CR. Gene Expression Profiling of Liposarcoma Identifies Distinct Biological Types/Subtypes and Potential Therapeutic Targets in Well-Differentiated and Dedifferentiated Liposarcoma. Cancer Research. 2007; 67:6626–6636. [PubMed: 17638873]

53. Taylor BS, Barretina J, Socci ND, Decarolis P, Ladanyi M, Meyerson M, Singer S, Sander C. Functional copy-number alterations in cancer. PloS one. 2008; 3:e3179. [PubMed: 18784837]

54. Czekanska EM. Assessment of cell proliferation with resazurin-based fluorescent dye. Methods in Molecular Biology. 2011; 740:27–32. [PubMed: 21468965]

55. Kaushik P, Molinelli E, Miller ML, Liu W, Wang W, Korkut A, Lu Y, Mills GB, Sander C. Spatial Normalization of Reverse Phase Protein Array Data. (Submitted).

56. Hu J, He X, Baggerly KA, Coombes KR, Hennessy BTJ, Mills GB. Non-parametric quantification of protein lysate arrays. Bioinformatics. 2007; 23:1986–1994. [PubMed: 17599930]

57. Pineda F. Generalization of back-propagation to recurrent neural networks. Physiological Review Letters. 1987; 59:2229–2232.

58. Pe'er D. Bayesian network analysis of signaling networks: a primer. Science STKE. 2005; 2005:pl4.

59. Sachs K, Perez O, Pe'er D, Lauffenburger DA, Nolan GP. Causal protein-signaling networks derived from multiparameter single-cell data. Science. 2005; 308:523–529. [PubMed: 15845847]

60. Schneider T, Kruse T, Wimmer R, Wiedemann I, Sass V, Pag U, Jansen A, Nielsen AK, Mygind PH, Raventos DS, Neve S, Ravn B, Bonvin AMJJ, De Maria L, Andersen AS, Gammelgaard LK, Sahl HG, Kristensen HH. Plectasin, a Fungal Defensin, Targets the Bacterial Cell Wall Precursor Lipid II. Science. 2010; 328:1168–1172. [PubMed: 20508130]

61. Persad S, Attwell S, Gray V, Mawji N, Deng JT, Leung D, Yan J, Sanghera J, Walsh MP, Dedhar S. Regulation of protein kinase B/Akt-serine 473 phosphorylation by integrin-linked kinase: critical roles for kinase activity and amino acids arginine 211 and serine 343. Journal of Biological Chemistry. 2001; 276:27462–27469. [PubMed: 11313365]

62. Gingras AC, Kennedy SG, O'Leary MA, Sonenberg N, Hay N. 4E-BP1, a repressor of mRNA translation, is phosphorylated and inactivated by the Akt(PKB) signaling pathway. Genes and Development. 1998; 12:502–513. [PubMed: 9472019]

63. Fang X, Yu SX, Lu Y, Bast RC, Woodgett JR, Mills GB. Phosphorylation and inactivation of glycogen synthase kinase 3 by protein kinase A. Proceedings of the National Academy of Sciences. 2000; 97:11960–11965.

64. Cantley LC, Neel BG. New insights into tumor suppression: PTEN suppresses tumor formation by restraining the phosphoinositide 3-kinase/AKT pathway. Proceedings of the National Academy of Sciences. 1999; 96:4240–4245.

65. Chung J, Uchida E, Grammer TC, Blenis J. STAT3 serine phosphorylation by ERK-dependent and -independent pathways negatively modulates its tyrosine phosphorylation. Molecular and Cellular Biology. 1997; 17:6508–6516. [PubMed: 9343414]

66. Dufner A, Andjelkovic M, Burgering BMT, Hemmings BA, Thomas G. Protein Kinase B Localization and Activation Differentially Affect S6 Kinase 1 Activity and Eukaryotic Translation Initiation Factor 4E-Binding Protein 1 Phosphorylation. Molecular and Cellular Biology. 1999; 19:4525–4534. [PubMed: 10330191]

67. Connell-Crowley L, Harper JW, Goodrich DW. Cyclin D1/Cdk4 regulates retinoblastoma protein-mediated cell cycle arrest by site-specific phosphorylation. Molecular Biology of the Cell. 1997; 8:287–301. [PubMed: 9190208]

68. Jorissen RN, Walker F, Pouliot N, Garrett TPJ, Ward CW, Burgess AW. Epidermal growth factor receptor: mechanisms of activation and signalling. Experimental Cell Research. 2003; 284:31–53. [PubMed: 12648464]

69. Yogi A, Callera GE, Montezano ACI, Aranha AB, Tostes RC, Schiffrin EL, Touyz RM. Endothelin-1, but not Ang II, Activates MAP Kinases Through c-Src–Independent Ras-Raf–Dependent Pathways in Vascular Smooth Muscle Cells. Arteriosclerosis, Thrombosis, and Vascular Biology. 2007; 27:1960–1967.

70. Beeser A, Jaffer ZM, Hofmann C, Chernoff J. Role of Group A p21-activated Kinases in Activation of Extracellular-regulated Kinase by Growth Factors. Journal of Biological Chemistry. 2005; 280:36609–36615. [PubMed: 16129686]

71. Rommel C, Clarke BA, Zimmermann S, Nuñez L, Rossman R, Reid K, Moelling K, Yancopoulos GD, Glass DJ. Differentiation stage-specific inhibition of the Raf-MEK-ERK pathway by Akt. Science. 1999; 286:1738–1741. [PubMed: 10576741]

72. Gosens R, Dueck G, Rector E, Nunes RO, Gerthoffer WT, Unruh H, Zaagsma J, Meurs H, Halayko AJ. Cooperative regulation of GSK-3 by muscarinic and PDGF receptors is associated with airway myocyte proliferation. Lung Cellular and Molecular Physiology. 2007; 293:L1348–L1358. [PubMed: 17873004]

73. Fedele M, Visone R, De Martino I, Troncone G, Palmieri D, Battista S, Ciarmiello A, Pallante P, Arra C, Melillo RM, Helin K, Croce CM, Fusco A. HMGA2 induces pituitary tumorigenesis by enhancing E2F1 activity. Cancer Cell. 2006; 9:459–471. [PubMed: 16766265]

74. Mohan S, Baylink D. IGF-binding proteins are multifunctional and act via IGF-dependent and -independent mechanisms. Journal of Endocrinology. 2002; 175:19–31. [PubMed: 12379487]

75. Mur C, Arribas M, Benito M, Valverde AM. Essential Role of Insulin-Like Growth Factor I Receptor in Insulin-Induced Fetal Brown Adipocyte Differentiation. Endocrinology. 2003; 144:581–593. [PubMed: 12538620]

76. Kuemmerle JR. Occupation of αvβ3-integrin by endogenous ligands modulates IGF-I receptor activation and proliferation of human intestinal smooth muscle. American Journal of Physiology. 2006; 290:G1194–G1202. [PubMed: 16195423]

77. Zhang W, Liu HT. MAPK signal pathways in the regulation of cell proliferation in mammalian cells. Cell Research. 2002; 12:9–18. [PubMed: 11942415]

78. Lehman JA, Gomez-Cambronero J. Molecular crosstalk between p70S6k and MAPK cell signaling pathways. Biochemical and Biophysical Research Communications. 2002; 293:463–469. [PubMed: 12054624]

79. Zheng CF, Guan KL. Activation of MEK family kinases requires phosphorylation of two conserved Ser/Thr residues. EMBO J. 1994; 13:1123–1131. [PubMed: 8131746]

80. Zheng CF, Guan KL. Cloning and characterization of two distinct human extracellular signal-regulated kinase activator kinases, MEK1 and MEK2. Journal of Biological Chemistry. 1993; 268:11435–11439. [PubMed: 8388392]

81. Dong G, Chen Z, Li ZY, Yeh NT, Bancroft CC, Van Waes C. Hepatocyte Growth Factor/Scatter Factor-induced Activation of MEK and PI3K Signal Pathways Contributes to Expression of Proangiogenic Cytokines Interleukin-8 and Vascular Endothelial Growth Factor in Head and Neck Squamous Cell Carcinoma. Cancer Research. 2001; 61:5911–5918. [PubMed: 11479233]

82. Coughlin S, Escobedo J, Williams L. Role of phosphatidylinositol kinase in PDGF receptor signal transduction. Science. 1989; 243:1191–1194. [PubMed: 2466336]

83. Scheid MP, Marignani PA, Woodgett JR. Multiple Phosphoinositide 3-Kinase-Dependent Steps in Activation of Protein Kinase B. Molecular and Cellular Biology. 2002; 22:6247–6260. [PubMed: 12167717]

84. Bornancin F, Parker PJ. Phosphorylation of protein kinase C-alpha on serine 657 controls the accumulation of active enzyme and contributes to its phosphatase-resistant state. Journal of Biological Chemistry. 1997; 272:3544–3549. [PubMed: 9013603]

85. Valovka T, Verdier F, Cramer R, Zhyvoloup A, Fenton T, Rebholz H, Wang ML, Gzhegotsky M, Lutsyk A, Matsuka G, Filonenko V, Wang L, Proud CG, Parker PJ, Gout IT. Protein Kinase C Phosphorylates Ribosomal Protein S6 Kinase βII and Regulates Its Subcellular Localization. Molecular and Cellular Biology. 2003; 23:852–863. [PubMed: 12529391]

86. Adams PD, Li X, Sellers WR, Baker KB, Leng X, Harper JW, Taya Y, Kaelin WG. Retinoblastoma Protein Contains a C-terminal Motif That Targets It for Phosphorylation by Cyclin-cdk Complexes. Molecular and Cellular Biology. 1999; 19:1068–1080. [PubMed: 9891042]

87. Volarevic S, Stewart MJ, Ledermann B, Zilberman F, Terracciano L, Montini E, Grompe M, Kozma SC, Thomas G. Proliferation, but not growth, blocked by conditional deletion of 40S ribosomal protein S6. Science. 2000; 288:2045–2047. [PubMed: 10856218]

88. Stover DR, Furet P, Lydon NB. Modulation of the SH2 Binding Specificity and Kinase Activity of Src by Tyrosine Phosphorylation within Its SH2 Domain. Journal of Biological Chemistry. 1996; 271:12481–12487. [PubMed: 8647855]

89. Xu W, Yuan X, Beebe K, Xiang Z, Neckers L. Loss of Hsp90 Association Up-Regulates Src-Dependent ErbB2 Activity. Molecular and Cellular Biology. 2007; 27:220–228. [PubMed: 17030621]

90. Haynes MP, Li L, Sinha D, Russell KS, Hisamoto K, Baron R, Collinge M, Sessa WC, Bender JR. Src Kinase Mediates Phosphatidylinositol 3-Kinase/Akt-dependent Rapid Endothelial Nitric-oxide Synthase Activation by Estrogen. Journal of Biological Chemistry. 2003; 278:2118–2123. [PubMed: 12431978]

91. Westwick JK, Bielawska AE, Dbaibo G, Hannun YA, Brenner DA. Ceramide Activates the Stress-activated Protein Kinases. Journal of Biological Chemistry. 1995; 270:22689–22692. [PubMed: 7559390]

92. Vindis C, Cerretti DP, Daniel TO, Huynh-Do U. EphB1 recruits c-Src and p52Shc to activate MAPK/ERK and promote chemotaxis. The Journal of Cell Biology. 2003; 162:661–671. [PubMed: 12925710]

93. Paulson M, Pisharody S, Pan L, Guadagno S, Mui AL, Levy DE. Stat protein transactivation domains recruit p300/CBP through widely divergent sequences. Journal of Biological Chemistry. 1999; 274:25343–25349. [PubMed: 10464260]

94. Toshio H, Katsuhiko I, Masahiko H. Roles of STAT3 in mediating the cell growth, differentiation and survival signals relayed through the IL-6 family of cytokine receptors. Oncogene. 2000; 19

95. Hara K, Maruki Y, Long X, Yoshino K-i, Oshiro N, Hidayat S, Tokunaga C, Avruch J, Yonezawa K. Raptor, a Binding Partner of Target of Rapamycin (TOR), Mediates TOR Action. Cell. 2002; 110:177–189. [PubMed: 12150926]

96. Ali SM, Sabatini DM. Structure of S6 Kinase 1 Determines whether Raptor-mTOR or Rictor-mTOR Phosphorylates Its Hydrophobic Motif Site. Journal of Biological Chemistry. 2005; 280:19445–19448. [PubMed: 15809305]

Figure 1.

Drug combination screen identifies synergistic and antagonistic drug targets in the dedifferentiated liposarcoma cell line, DDLS8817. (**A**) Example of CI score calculation of paired drug perturbation using the MEK inhibitor, SL327 (MEKi), and the AKT inhibitor, AKT inhibitor VIII (AKTi). Cell viability was estimated after 72 hours of drug treatment by the Resazurin assay that measures cellular metabolic activity. Error bars represent standard deviation of at least four biological replicates. (**B**) CI scores for a drug synergy screen performed in DDLS8817 cells using 14 targeted inhibitors ("Inh" or "i" in the labels). CI scores were derived as described in (**A**) and categorized as synergistic (<0.75, red), antagonistic (>1.5, blue), or additive (green). In some cases CI scores could not be calculated (gray). Inset shows distribution of CI scores. A complete list of targets and secondary targets of the drugs used are provided in table S1. Each CI score represents data from seven different drug doses of single and paired drug treatments with at least four biological replicates per condition.
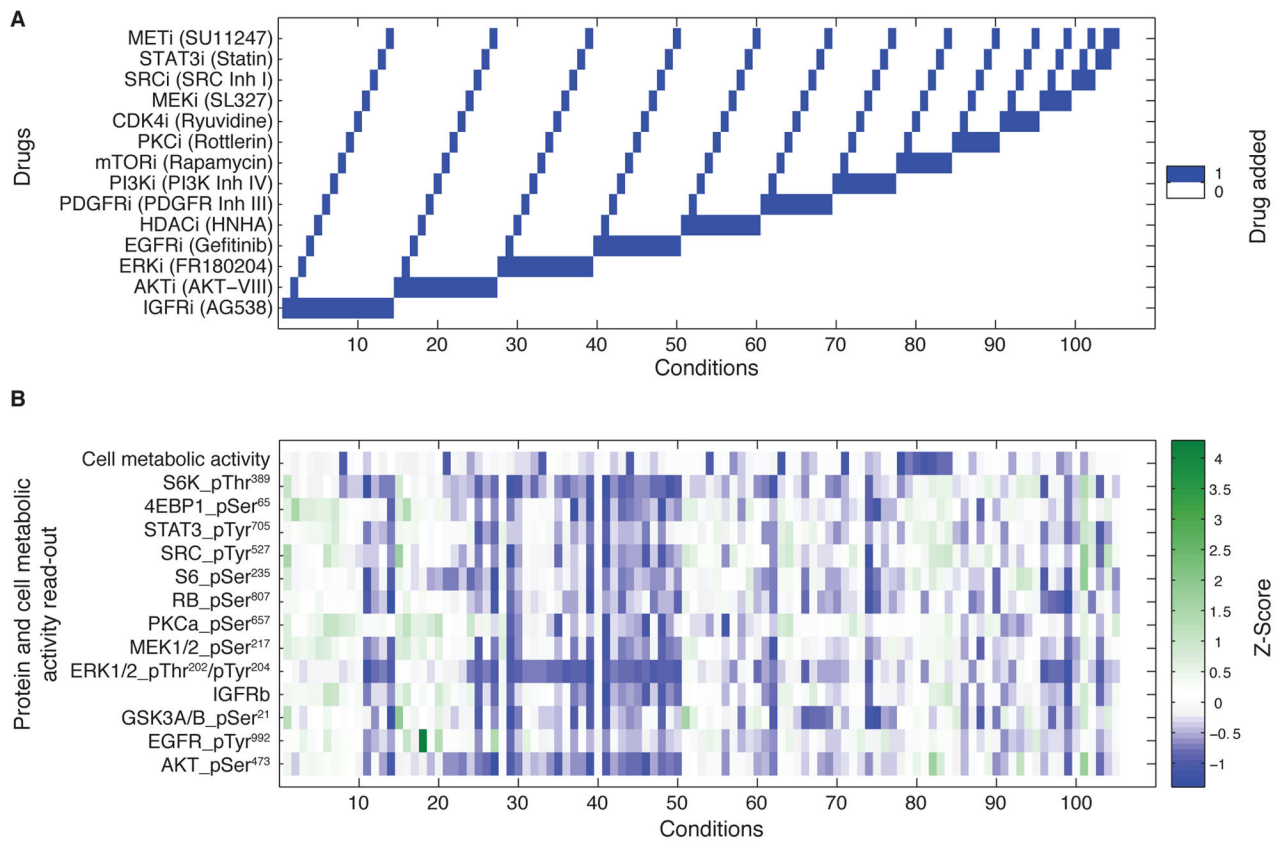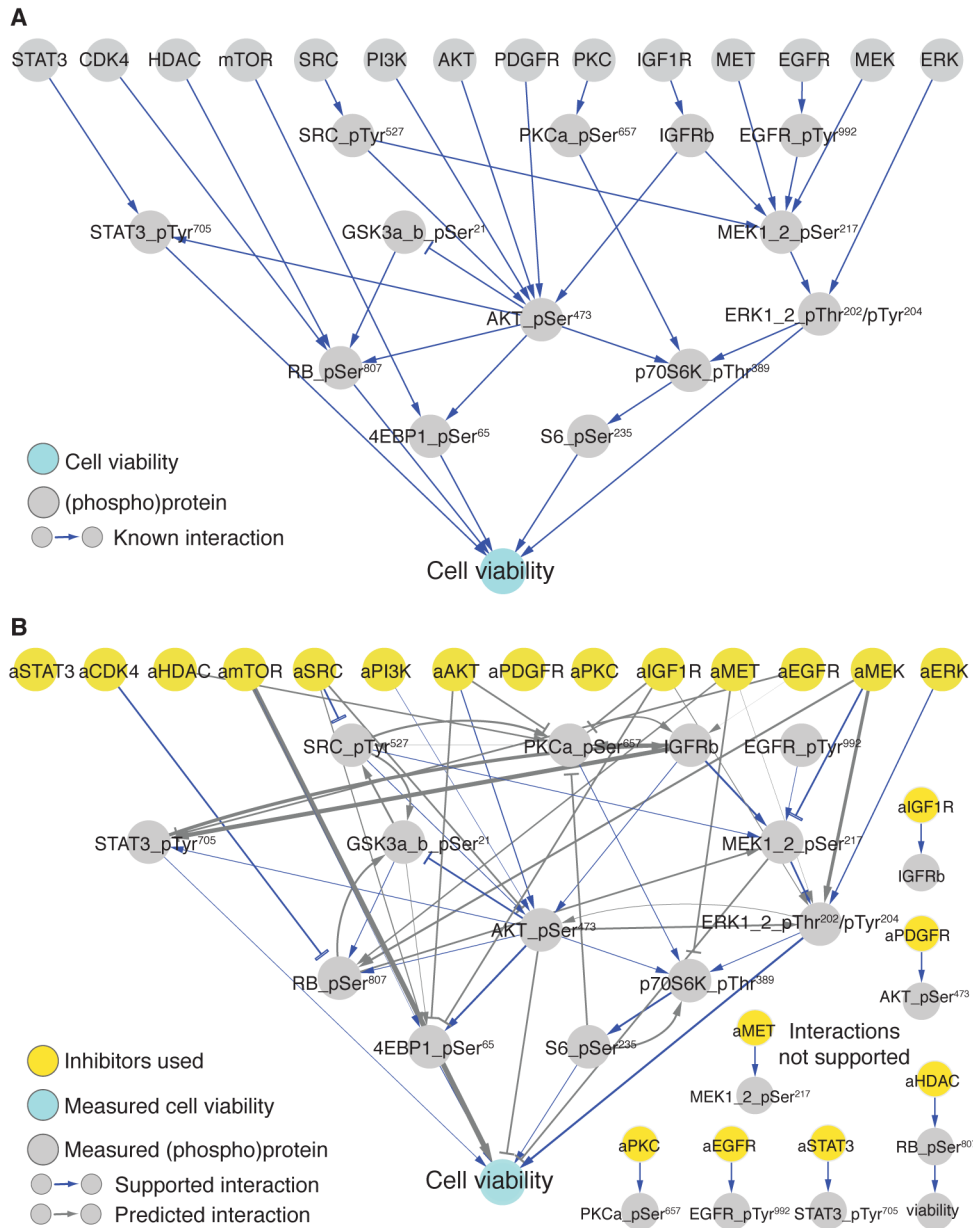
Figure 2.
IGF1R and CDK4 are synergistic drug targets in DDLS. **(A)** Dose-response effects of the CDK4 inhibitor PD0332991 and the IGF1R antibody R1507 on inhibition of cell viability in DDLS8817 cells estimated after six days of drug treatment using the CCK-8 assay that measures cell metabolic activity (upper panel). Each condition represents at least four biological replicates. CI scores were calculated at various effects (lower panel). **(B)** Performed as in **(A)** in the DDLS cell line LPS141.

Figure 3.
Systematic drug treatments and large-scale proteomic profiling in DDLS8817. **(A)** Experimental design of 14 individual and 91 pairwise drug perturbations with a set of targeted small molecule drugs. **(B)** Response of 13 proteins or phosphoproteins [phosphorylated at the indicated residue(s)] after 24 hours of drug treatment as shown in **(A)** assessed by RPPA. The effect on cell viability was estimated with the resazurin assay (measures cell metabolic activity) after 72 hours of drug treament. All read-outs were z-score normalized. Each condition represents the mean of two biological replicates.

Figure 4.
Network inference of proteomic data profiles and prior knowledge interactions provides signaling models specific to DDLS. **(A)** A network of prior knowledge interactions (edges) between the selected set of protein read-outs (nodes) measured by RPPA and their connection to cell viability, as measured by metabolic activity assays in Fig. 3B. **(B)** Inferred network models from perturbation-response data and prior knowledge information with the line width reflecting the most probable interactions. The network represents the average network of the 100 lowest error models. Predicted interactions (gray) and prior knowledge interactions that are retained (blue) and rejected are indicated. Nodes that are perturbed but not observed are termed "activity node" and preceded by an "a" (for example, aAKT) and represent the presumed, direct target of the drugs applied.
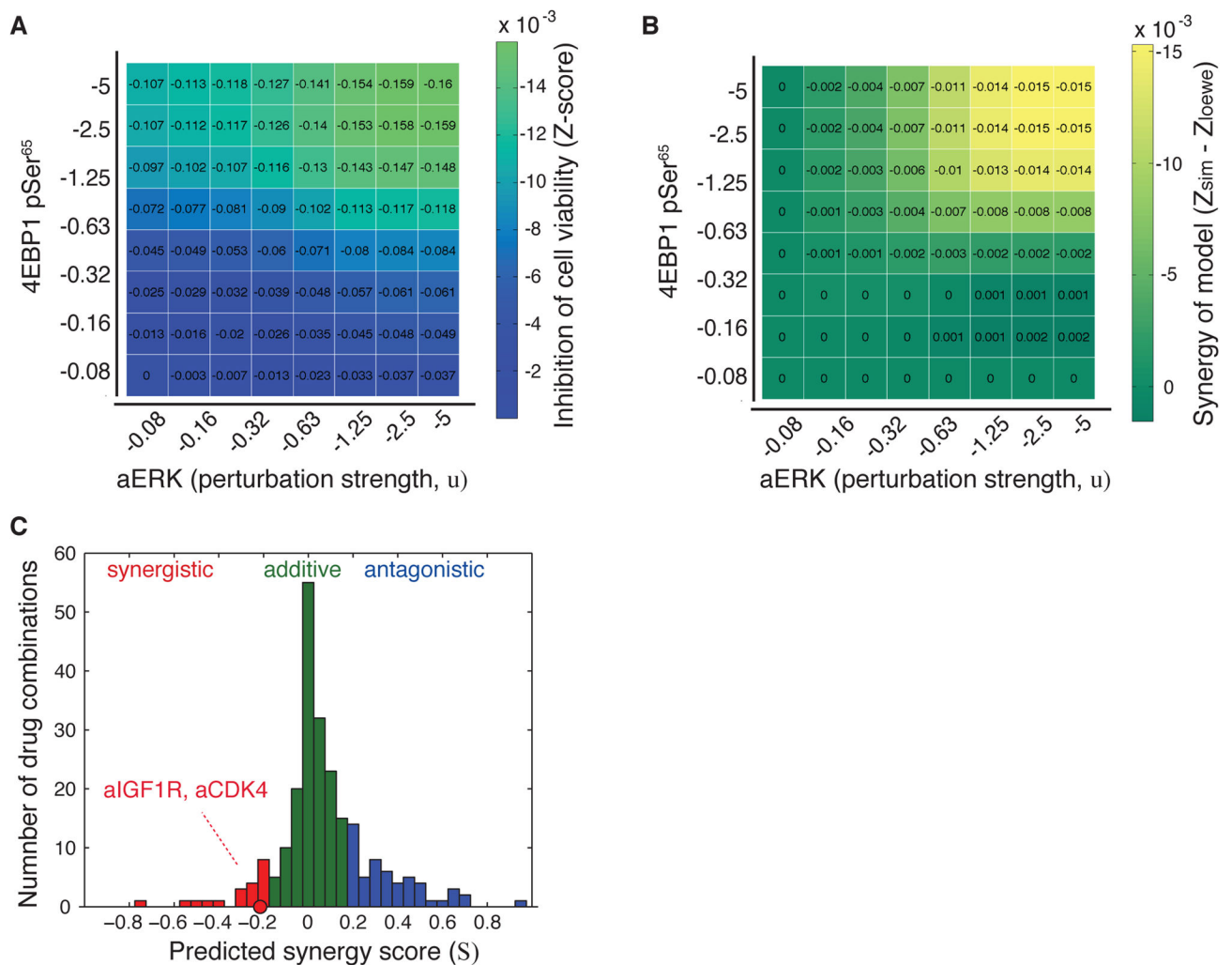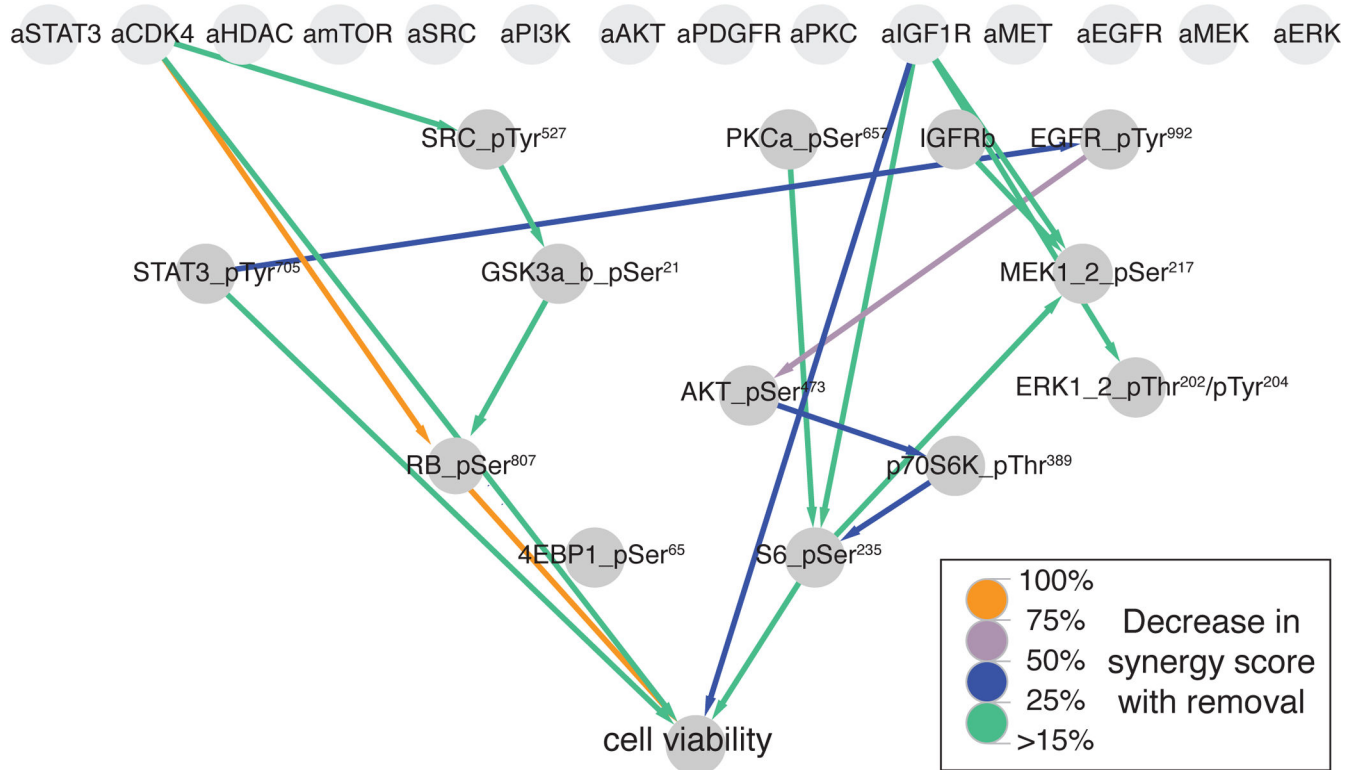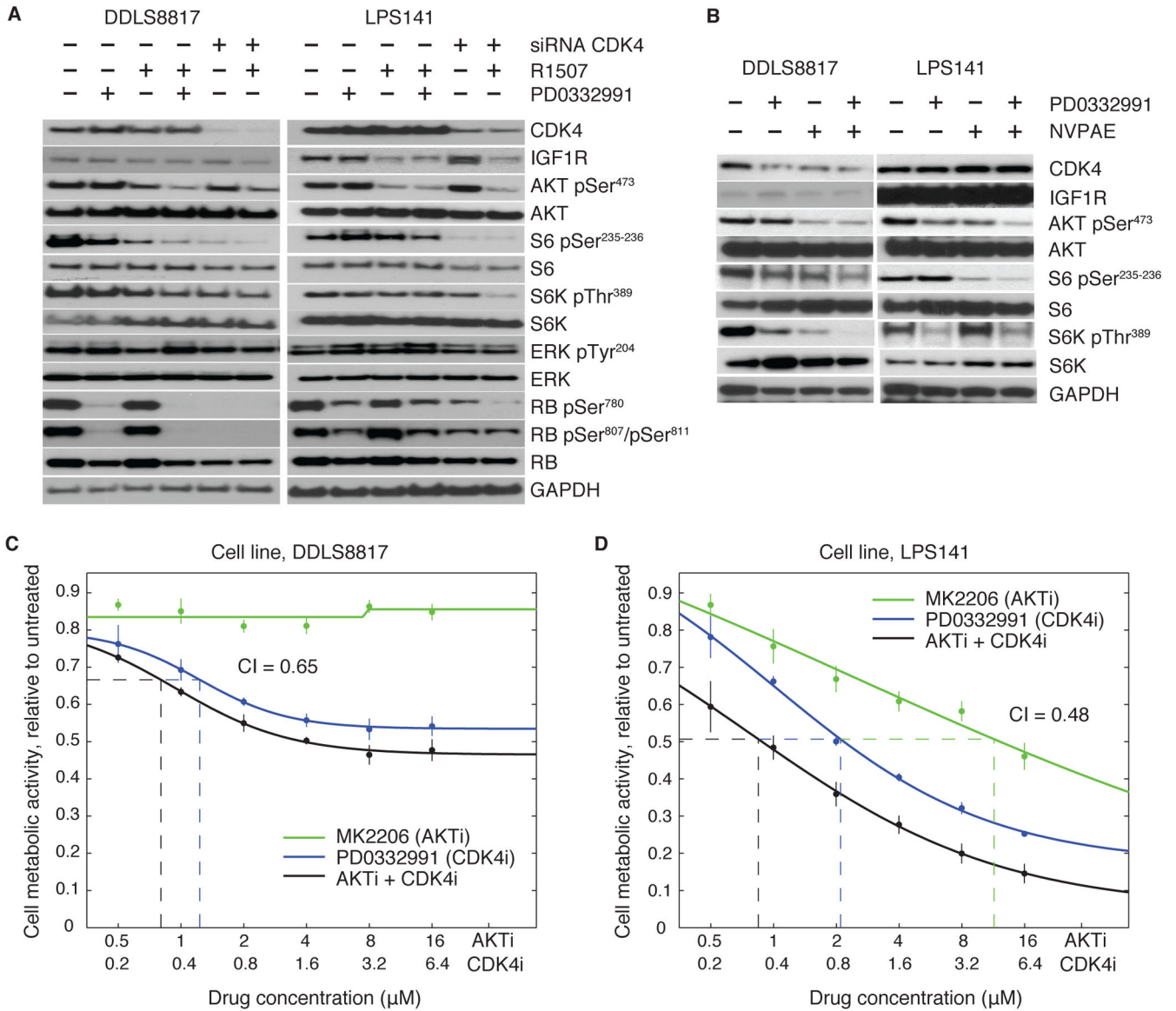
Figure 5.
Synergistic effects are captured in the network models, and the experimentally observed CDK4-IGF1R drug synergy is recapitulated. **(A)** Example of calculation of model-based synergy scores (S) by *in silico* perturbation of the 4EBP1_pSer[65] (pholphorated at Serine 65) and ERK encoded as an activity node (aERK, external drug node). These nodes were inhibited with eight different perturbation strengths (u) in all possible combinations and the effect was recorded as the response on the cell viability node (z-score). **(B),** Non-additive synergy effects (Synergy of model) were determined as the difference between the effect of the paired inhibition and the added effects of the two single node inhibitions ($S=-0.24$ for aERK and 4EBP1_pSer[65]). **(C),** Computed synergy scores for all node-pairs where each synergy scores was determined from 64 unique perturbations as in (**A**). Synergy scores were categorized into three classes, where $S<-0.20$ was considered synergistic (red), >0.20 antagonistic (blue), and otherwise additive (green). The synergy score for IGF1R and CDK4 node inhibition is highlighted ($S=-0.23$).

Figure 6.
Simulation of information flow in network models predicts several important interactions mediating the synergy of CDK4 and IGF1R inhibition, including AKT pathway members. Network edges ranked by their contribution to the model-simulated synergy between CDK4 and IGF1R inhibitors. Each edge was removed in turn and the effect on the cell viability synergy score was recalculated and expressed as the percent suppression of original synergy score. The leave-edge-out calculations were performed using the 100 lowest error models.

Figure 7.
The AKT pathway is likely involved in the synergy of CDK4 and IGF1R inhibitors. **(A)** Western blot of DDLS8817 and LPS141 cells inhibited for 12 hours with 10 μg/mL R1507 (IGF1R antibody), 1uM PD0332991 (CDK4 inhibitor), and siRNA-mediated knockdown of CDK4. **(B)** Similar to (**A**), except cells were inhibited for 24 hours with 1 μM NVP-AEW541 (IGF1R inhibitor) and PD0332991. Western blots shown are representative data of at least two independent experiments. **(C)** Dose-response measurements of cell metabolic activity using the CCK-8 assay (correlates with cell viability) of DDLS8817 cells after drug treatment for 6 days with the AKT inhibitor MK2206 and the CDK4 inhibitor PD0332991. The combination index (CI) score is indicated and was determined at EC50 levels indicated by dashed lines. Error bars represent standard deviation of six biological replicates. **(D)** Similar to (**C**) but in LPS141 cells.